# Radiative recombination of trapped excitons in $Alq_3$ films: Importance of intermolecular interactions

A. M. Ajward,[1] X. Wang,[1] N. Wickremasinghe,[1] L. A. A. DeSilva,[2] and H. P. Wagner[1,*]
[1]*Department of Physics, University of Cincinnati, Cincinnati, Ohio 45221, USA*
[2]*Department of Physics, University of West Georgia, Carrollton, Georgia 30118, USA*
(Received 17 December 2012; revised manuscript received 3 May 2013; published 23 July 2013)

We investigate the light emission of optically excited tris(8-hydroxyquinolinato) aluminum ($Alq_3$) films by temperature-dependent, time-integrated, as well as time-resolved photoluminescence (PL) at various photon densities. The $Alq_3$ films are deposited on Si (001) substrate using organic molecular beam deposition. At high excitation densities, the PL efficiency decreases when the temperature is reduced from 170 to 15 K. At low laser intensities, the PL efficiency is nearly temperature independent. The observed PL quenching at high-excitation densities is assigned to singlet-singlet annihilation revealing a low-temperature bimolecular quenching coefficient that is more than two orders of magnitude higher than previously reported at room temperature. The observed strong bimolecular interaction at low temperature is attributed to an enhanced local (microscopic) density of captured excitons in extended traps. The reduction of the exciton annihilation with increasing temperature is assigned to a thermally activated occupation of nonquenchable localized exciton states. Above 190 K, the PL efficiency starts to decrease independently from the excitation level which is ascribed to a thermally activated detrapping of excitons and subsequent migration to nonradiative centers outside the traps. A coupled-rate equation model, including bimolecular quenching, thermally activated occupation of nonquenchable states, and detrapping of excitons at higher temperatures, supports these interpretations.

DOI: 10.1103/PhysRevB.88.045205 PACS number(s): 78.55.Kz, 78.66.Qn, 78.47.jd

## I. INTRODUCTION

The demonstration of electroluminescence (EL) from tris(8-hydroxyquinolinato) aluminum ($Alq_3$)–based organic light-emitting diodes (OLEDs) in 1987[1] has initiated significant research interest[2–5] in OLEDs that are now available on the market. $Alq_3$ films are still frequently used as an efficient emissive layer in such structures. Presently, the external quantum efficiency $\eta_{EL}$ of $Alq_3$-based OLEDs reaches $\sim$8%,[6] which is subject to progressing improvements by using different carrier transport layers and device architecture as well as by improving the carrier injection.[6–13] In addition, layer deposition at different growth conditions and film annealing[14–20] lead to an enhancement of device lifetime and to an increase of the quantum efficiency, which has been attributed to a morphology change in the quasiamorphous $Alq_3$ films. However, the interplay between short-range crystalline ordered and disordered regions in the vicinity of grain boundaries and the influence of interacting molecules on recombination processes in $Alq_3$-based OLEDs are still rather unexplored.

$Alq_3$ crystallizes in five different polymorphic phases ($\alpha$, $\beta$, $\gamma$, $\delta$, and $\varepsilon$), which can occur in meridional and facial stereoisomers.[21–26] Photoluminescence (PL) studies of polycrystalline $\alpha$ and $\beta$ $Alq_3$ samples[21–23] reveal an emission spectrum with vibronic progression. The vibronic mode separation energy of 64 meV has been attributed to three intense skeletal in-plane bending modes of the quinoxaline ligand. Density functional theoretical[27] calculations support this interpretation. No vibronic progression has been observed in the PL spectrum of $Alq_3$ thin films,[21–23] which is explained by the polymorphous structure of the films that contain all possible crystalline modifications on a small (several tens of nanometers) length scale. This disorder causes a vast distribution of crystalline environments, resulting in a large inhomogeneous broadening of the vibronic subbands. Moreover, it causes both extended and isolated potential minima below the mobile Frenkel exciton energies,[28,29] which are caused by compressive strain[30] and the changing molecular environment when different molecular ordered regions morph into another. Optically excited mobile Frenkel excitons, which are generated in regions of higher molecular order, relax via directed exciton diffusion into these energy traps. Accordingly, the PL of trapped excitons in $Alq_3$ films is redshifted by approximately 100 meV (at 4 K) compared to the Frenkel exciton emission in bulk crystals.[21,22] The small interligand separation of 0.35 to 0.39 nm in $\alpha$ and $\beta$ $Alq_3$ crystals,[21] respectively, and of 0.34 nm in $\varepsilon$ $Alq_3$ (Ref. 25) may also enable the formation of charge-transfer (CT)-like exciton states, where the electronic excitation is shared between two adjacent ligands of different molecules. Such CT states, which are either polar CT excitons or neutral excimers, have been extensively studied in 3,4,9,10-perylene tetracarboxylic dianhydride ($\alpha$-PTCDA) crystals[31,32] and in polycrystalline PTCDA films,[33,34] where the stacked molecular distance is 0.32 nm.

Since different types of trapped excitons including CT-like states are similar in energy, it is difficult to discriminate the emission of these states by conventional spectrally resolved PL. Temperature-dependent PL experiments provide additional information since the emission intensity changes as a function of thermally activated state occupation. Time-resolved PL (TRPL) techniques can also discriminate among different types of excitonic transitions because of their diverse radiative lifetimes. In addition, intensity-dependent TRPL measurements allow identifying singlet-singlet annihilation at higher exciton densities.

A variety of temperature-dependent PL or TRPL experiments have been performed on pure $Alq_3$ films. However, due to dissimilar experimental conditions, the results and interpretations of these investigations are mostly different from each other. Recent temperature-dependent PL studies on

 

90-nm-thick $Alq_3$ films[35] fabricated by vacuum evaporation reveal an increase of the PL efficiency when the temperature is increased from 15 to 190 K, while the PL efficiency starts to decrease at temperatures above 190 K. The observed PL enhancement between 15 and 190 K has been attributed to an increasing number of thermally activated, intermolecular, delocalized Frenkel excitons with a high emission rate. The PL decrease at higher temperatures is ascribed to thermal activation of intramolecular delocalized CT excitons. In contrast with these investigations, spectrally integrated TRPL studies[36–39] on $\sim$1-$\mu$m-thick $Alq_3$ films on quartz, using a frequency-tripled YAG laser with high photon densities, reveal a monotonously decreasing PL intensity when the temperature is increased from 70 to 300 K. In addition, a single exponential PL decay time decreasing from 20 to 16 ns has been observed as a function of rising temperature. The decrease of the PL intensity and decay time with increasing temperature has been attributed to an enhanced migration of excitons to nonradiative (NR) defects. Spectrally and time-resolved experiments on a 150 nm $Alq_3$ film on quartz at 300 K reveal a multiexponential PL decay[40] originating from short-lived emissive centers in shallow traps with 1–20-ps lifetime and from deeply ($\sim$200 meV) trapped excitons with a lifetime of $\sim$10 ns. Further time-resolved studies[41] assign the occurrence of two decay times in the PL trace ($\sim$2 and $\sim$10 ns) to the recombination of trapped excitons from facial and meridional isomers in the $Alq_3$ film.

Different results were also reported for singlet-singlet annihilation processes at high optical excitation densities.[38,39,42,43] Recent studies on a 100-nm-thick $Alq_3$ film fabricated by high-vacuum deposition using a cw Ar ion at an average excitation energy of 3.46 eV at 300 K[43] reveal an annihilation constant of $(1.1 \pm 0.5) \times 10^{-10}$ $cm^3s^{-1}$, which is a factor of three higher than the value of $(3.5 \pm 2.5) \times 10^{-11}$ $cm^3s^{-1}$ obtained in Ref. 39. Further investigations[38,42] at 300 and 77 K reveal quenching constants of $(8 \pm 2.5) \times 10^{-12}$ $cm^3s^{-1}$ and $(4 \pm 2) \times 10^{-12}$ $cm^3s^{-1}$, respectively, thus more than one order of magnitude lower than reported by Ref. 43.

In this paper, we investigate the emission of thin $Alq_3$ films grown on Si (001) by temperature-dependent, time-integrated, or time-resolved PL spectroscopy at different excitation densities. The goal of these investigations is to identify different recombination channels that contribute to the total light emission in order to provide a more comprehensive understanding of the relaxation and recombination dynamics of optically excited $Alq_3$ films. The observed temperature dependence of the $Alq_3$ emission is described in Secs. III A and III B. Our experiments indicate that the PL at low temperature (15 to 100 K) predominantly originates from excitons in extended traps possessing a high local (microscopic) exciton density, thus revealing singlet-singlet annihilation already at moderate excitation levels. At higher temperatures, thermally activated nonquenchable exciton states contribute to the radiative emission. These nonquenchable states may include excitons in isolated traps and CT-like excitons. A rate equation model, which is explained in Sec. IV supports these interpretations.

## II. EXPERIMENTAL DETAILS

The $Alq_3$ films were grown by organic molecular beam deposition (OMBD) at room temperature. Chemically clean $n$-type (001)-oriented Si wafers were used as substrates. The Si substrates were cleaned successively in acetone, methanol, and ultrapure water using an ultrasonic bath. Immediately after cleaning, the substrates were transferred into the high-vacuum OMBD chamber with a base pressure of $10^{-8}$ mbar. The $Alq_3$ source material (Sigma Aldrich) was purified by sublimation under high vacuum ($10^{-6}$ mbar) at a temperature of 210 °C before it was placed in the Knudsen cells. The deposition rate of 0.01 nm/s at the growth temperature of 230 °C was determined by a calibrated quartz crystal-thickness monitor. After the film deposition, the samples were quickly transferred into an evacuated temperature-variable cryostat to minimize the exposure of the $Alq_3$ films to atmospheric water and oxygen.

For time-integrated PL measurements, the $Alq_3$ films were excited by a cw GaN-based laser diode at $\sim$3.04 eV ($\lambda$ = 407 nm). The excitation power was varied between approximately 1 $\mu$W and 1 mW. For spectrally resolved PL measurements, a lens with a focal length of 300 mm was used to collimate the 2.5 mm diameter wide laser beam onto the sample, resulting in an excitation area of $30.4 \times 10^{-6}$ $cm^2$ on the film [see Eq. (11)]. Subsequently, the $Alq_3$ emission was analyzed in a spectrometer with a GaAs photomultiplier as detector.

For TRPL measurements, the $Alq_3$ film was excited by a frequency-doubled Ti:sapphire laser. The laser produces 100 fs laser pulses at a repetition rate of 80 MHz. The lifetime of trapped excitons in $Alq_3$ films has been found to be in the range of 10 to 25 ns.[36,41,44] In order to allow the excited system to relax back to the highest occupied molecular orbital (HOMO), the pulse repetition rate was reduced from 80 to 4 MHz (or $\sim$250 ns repetition time) by an acousto-optic pulse selector. The contrast ratio of the first-order diffracted pulses compared to the blocked zero-order pulses was better than $\sim$100. Subsequently, the laser pulses were frequency-doubled by a $BaB_2O_4$ (BBO) crystal to generate pulses with an excitation wavelength of $\lambda = 407$ nm ($\sim$3.04 eV), leading to a contrast ratio of the first-order diffracted pulses compared to the blocked zero-order pulses higher than 10 000. The average power of the light pulses has been varied between 10 and 300 $\mu$W. For the TRPL measurements, a lens with a focal length of 250 mm was used to collimate the 3.0 mm diameter wide pulsed laser beam onto the sample, resulting in a excitation area of $14.6 \times 10^{-6}$ $cm^2$ on the film. Time-resolved decay traces were recorded using the technique of time-correlated single-photon counting (TCSPC) with a response time of less than 2.5 ns. A closed-cycle He cryostat was used for variable temperature measurements between 15 and 300 K.

## III. EXPERIMENTAL RESULTS

### A. Time-integrated photoluminescence using cw excitation

The inset of Fig. 1 shows the PL spectra for different temperatures as labeled at a light energy of 3.04 eV and an excitation intensity of 3.6 W/$cm^2$. As previously observed by other groups,[21,23] the PL spectra do not show a vibronic progression. Instead, the PL reveals a broad emission band, which is attributed to the polymorphous growth of an $Alq_3$ film containing all possible crystalline modifications[21–26] within short-range ordered areas. At 15 K, the peak position of the PL spectrum ($\sim$2.385 eV) is shifted by approximately 100 meV

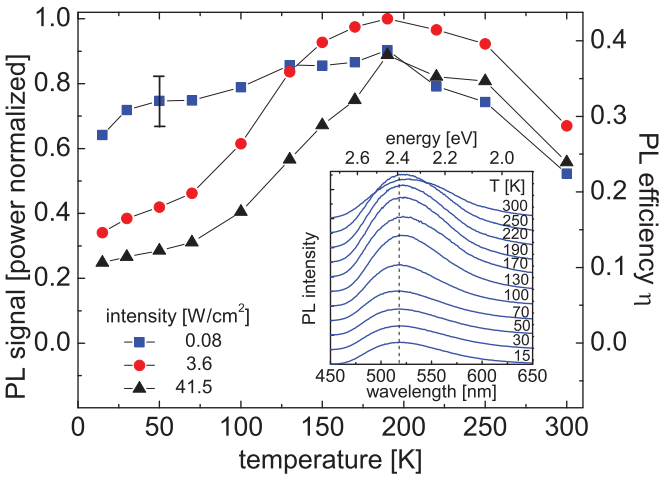


FIG. 1. (Color online) Power-normalized temperature-dependent and spectrally integrated PL efficiency of a 120-nm-thick $Alq_3$ film deposited on Si (001) at different excitation intensities as labeled. The $Alq_3$ film was excited using a cw GaN laser at an energy of 3.04 eV. Inset: PL spectra at an intensity of 3.6 W/cm$^2$ at different temperatures as labeled. The vertical dashed line is a guide for the eye.

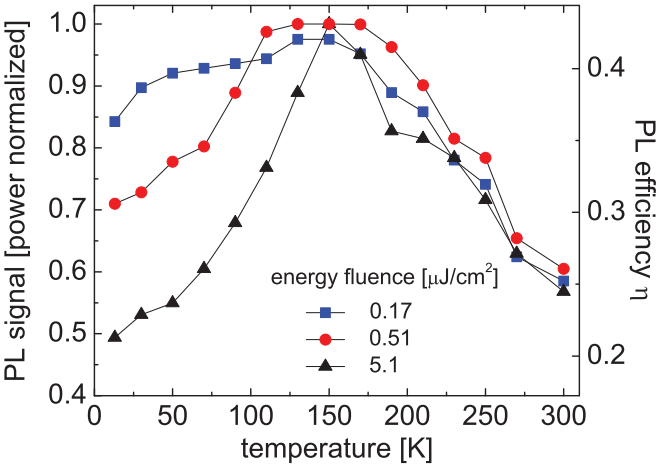


FIG. 2. (Color online) Temperature dependence of the time-integrated PL efficiency of a 120-nm $Alq_3$ film excited with 100 fs pulses at an energy of 3.04 eV at three different energy fluences per pulse as labeled. The PL signal has been detected at an energy of 2.32 eV.

to lower energies compared to the PL peak position obtained from $\alpha$ and $\beta$ $Alq_3$ polycrystalline samples, predominantly revealing Frenkel exciton emission.[21,23] The observed redshift compared to crystalline $Alq_3$ emission is attributed to the trapping energy of Frenkel excitons in the disordered $Alq_3$ film. From 15 to 190 K, the PL peak intensity increases by a factor of approximately three, and the emission maximum shifts by approximately 25 meV to lower energies. Above 190 K, the PL intensity decreases and the band maximum further shifts to lower energies.

The spectrally integrated intensity of the PL spectra at an excitation intensity of 3.6 W/cm$^2$ as a function of temperature is shown in Fig. 1. The measured PL intensities for very low (0.08 W/cm$^2$) and high (41.5 W/cm$^2$) excitation intensities are also displayed. For comparison, each of the spectrally integrated PL signals obtained at different excitation intensities has been divided by the incident laser power and subsequently normalized with respect to the highest PL signal value obtained at 190 K at an excitation intensity of 3.6 W/cm$^2$. The corresponding power-normalized PL signal as a function of temperature for different excitation intensities is shown on the left $y$ axis. Furthermore, the power-normalized PL intensities at 300 K obtained at different excitation intensities have been averaged and associated with a PL efficiency of $\eta \sim 0.25$ obtained by other groups.[45–47] The efficiency values as a function of temperature for different excitation intensities are correspondingly given on the right $y$ axis. Experimental uncertainties due to temperature or laser power fluctuations at a specific excitation intensity and systematic errors are estimated to be approximately 10% (see error bar in Fig. 1).

Our experimental result at an intensity of 3.6 W/cm$^2$ is similar to the temperature dependence that has been observed earlier in an $Alq_3$/PTCDA multilayer structure[34] and in a 90-nm-thick $Alq_3$ film observed by a different group.[35] At highest light intensity (41.5 W/cm$^2$), the PL efficiency decrease at low temperature is stronger compared to the observed reduction at 3.6 W/cm$^2$. At very low excitation intensity (0.08 W/cm$^2$), the quenching of the PL intensity is significantly reduced, and the PL efficiency at 15 K is nearly as high as at 190 K.

### B. Time-integrated and time-resolved PL measurements using pulsed excitation

To gain more information about the origin of the temperature and intensity dependence of the light emission in $Alq_3$ films, we performed experiments with pulsed laser excitation using 100 fs pulses at a photon energy of 3.04 eV. The time-integrated PL signal has been recorded at a detection energy of 2.32 eV for three energy fluences of 5.1, 0.51, and 0.17 $\mu$J/cm$^2$ per pulse. Figure 2 shows the temperature-dependent emission of a 120-nm-thick $Alq_3$ film. As in Fig. 1, the PL intensities have been power normalized, and the averaged power-normalized value at 300 K has been correlated with an efficiency value of $\eta \sim 0.25$. At an incident energy fluence of 0.17 $\mu$J/cm$^2$ per pulse, the PL efficiency shows nearly no temperature dependence when the temperature is lowered from 170 to 15 K, which is consistent with the low-intensity cw experiments in Fig. 1. At highest excitation density (5.1 $\mu$J/cm$^2$ fluence per pulse), the PL efficiency at 15 K is reduced by a factor of $\sim$2 compared to the value obtained at 170 K. Compared to the cw experiments, the PL efficiency maximum at pulsed laser excitation occurs at an approximately 20 K lower temperature, which is attributed to a transient local temperature increase in the sample at pulsed excitation condition.

The significant change of the PL efficiency in $Alq_3$ films at different intensities has been further studied using TRPL experiments at 2.32 eV detection energy. Figure 3 shows the power-normalized TRPL traces of a 120-nm-thick $Alq_3$ film at 15 K and at photon fluences of 5.1 and 0.17 $\mu$J/cm$^2$. At a high excitation density, the PL shows a pronounced nonexponential decay, and the initial signal close to zero decay time is reduced by approximately 10% compared to the signal obtained at low

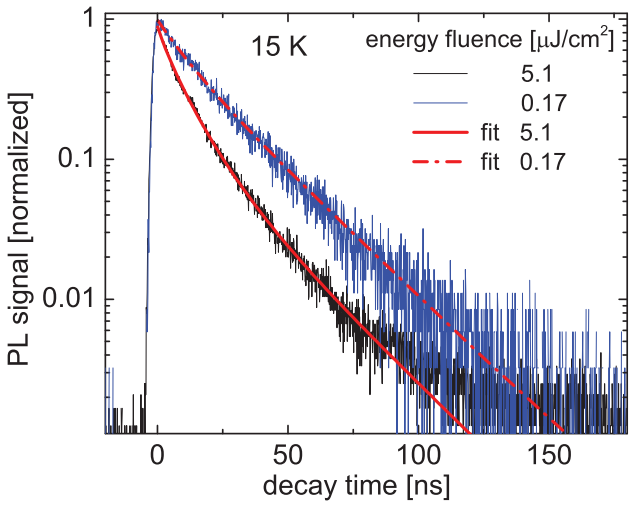


FIG. 3. (Color online) TRPL and power-normalized PL signal obtained from a 120-nm $Alq_3$ film at 15 K for two different energy fluences as labeled. Also shown as thick full and dashed red lines are biexponential fits including singlet-singlet annihilation as described in Sec. IV.

fluence. Both findings indicate that singlet-singlet annihilation processes are responsible for the observed PL efficiency drop at high excitation densities.

Figure 4 shows a waterfall diagram of PL traces obtained at temperatures ranging from 15 to 300 K when the $Alq_3$ film has been excited at an energy fluence of 5.1 $\mu J/cm^2$. For better visibility, the traces are offset with respect to each other. The measurements show that singlet-singlet annihilation is significantly reduced when the temperature increases from 15 to 170 K, resulting in a nearly single-exponential trace with

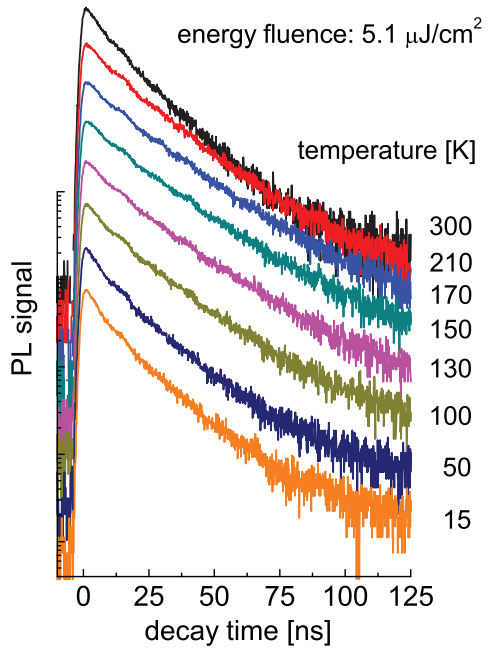


FIG. 4. (Color online) Power-normalized PL traces obtained from a 120-nm $Alq_3$ film at an incident energy fluence of 5.1 $\mu J/cm^2$ per pulse and different temperatures as labeled. The PL traces are detected at 2.32 eV. For better comparison, the traces are offset.

slightly longer decay times. Above 170 K, the decay traces remain nearly single exponential but show a reduced decay time, which is attributed to a thermally activated detrapping of radiatively recombining excitons and their subsequent migration to NR traps. The PL traces observed at fluences of 0.51 and 0.17 $\mu J/cm^2$ (not shown) reveal much less and nearly no temperature dependence, respectively, when the temperature is raised from 15 to 170 K, while the PL efficiency at temperatures above 170 K decreases as for high excitation densities.

## IV. INTERPRETATION OF THE EXPERIMENTAL RESULTS AND MODEL CALCULATIONS

### A. Singlet-singlet annihilation

To explain the observed bimolecular quenching at 15 K and the temperature dependence at higher temperatures, we consider that the excited Frenkel excitons in $Alq_3$ nanocrystals quickly relax via vibronic transitions (on a scale of a few hundreds of femtoseconds) into their lowest unoccupied molecular orbital (LUMO) $n = 0$ vibronic state. These relaxed "quasifree" Fenkel excitons migrate within the nanocrystal via intersite transport until they get trapped in deep potential minima at the grain boundaries between different $Alq_3$ nanocrystals. The trapping energies of these potential minima are estimated to be ~100 meV by comparing the PL maximum obtained from $\alpha$ $Alq_3$ crystals at 2.47 eV with the PL maximum obtained from an $Alq_3$ film at 2.36 eV (see Refs. 21–23).

For simplicity, we approximate the observed nonexponential PL decay of these trapped states to be biexponential, originating from two different and locally separated radiative centers $S_1$ and $S_2$ with exciton densities $n_1(t)$ and $n_2(t)$, neglecting any weak radiation from longer living states (see also Fig. 5). We attribute $S_1$ traps to disordered or defective areas, e.g., formed by compressive strain in the grain boundary between less ordered $Alq_3$ nanocrystals, which contain radiative as well as strongly disturbed or defective NR molecules.

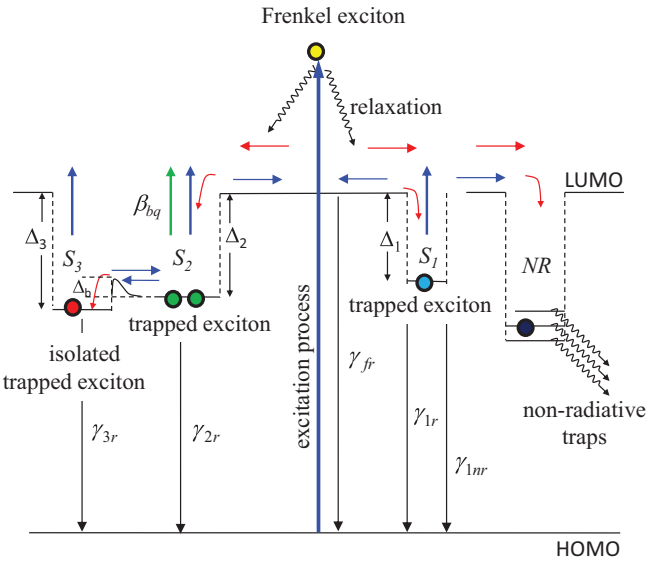


FIG. 5. (Color online) Sketch of the energy levels of exciton trapping sites and of radiative and NR processes in optically excited $Alq_3$ films as described in the text.

The $S_2$ trapping sites are attributed to more ordered and much less defective areas between adjacent ordered nanocrystals, which basically contain no NR centers. We therefore neglect nonradiative processes for $S_2$ excitons and approximate the measured $S_2$ lifetime to be essentially equal to the radiative lifetime of quasifree Frenkel excitons. All NR decays during the exciton filling process of $S_1$ and $S_2$ trapping sites are ascribed to NR centers outside the $S_1$ and $S_2$ trapping sites. Such NR centers, which also include triplet states,[48] are predominantly responsible for the reduction of the PL quantum yield in $Alq_3$ films to $\eta \sim 0.25$ at room temperature.[45–47] States $S_1$ and $S_2$ as well as NR centers are quickly filled (within a few hundreds of picoseconds) by the quasifree Frenkel excitons. When the film is excited at a low fluence of 0.17 $\mu J/cm^2$, bimolecular annihilation is strongly suppressed. Accordingly, densities $n_1(t)$ and $n_2(t)$ of states $S_1$ and $S_2$ approximately obey the equations (neglecting the state filling time):

$$n_1(t) = n_1(0)\exp(-t/\tau_1), \tag{1}$$

$$n_2(t) = n_2(0)\exp(-t/\tau_2). \tag{2}$$

The rate of the emitted photon density describing the time-resolved PL traces is given by

$$\begin{aligned} N_{\text{photon}}(t) &= \gamma_{1r} n_1(t) + \gamma_{2r} n_2(t) \\ &= \gamma_{1r} n_1(0)\exp(-t/\tau_1) + \gamma_{2r} n_2(0)\exp(-t/\tau_2) \\ &= A_1\exp(-t/\tau_1) + A_2\exp(-t/\tau_2). \end{aligned} \tag{3}$$

The thick dashed red line in Fig. 3 shows the fit of the low-power PL trace, revealing decay times of $\tau_1 = 1/\gamma_1 = 10 \pm 2$ ns and $\tau_2 = 1/\gamma_2 = 23 \pm 2$ ns. The lifetime $\tau_2 = \tau_{2r}$ of the purely radiative $S_2$ excitons (which is equal to the radiative lifetime of quasifree Frenkel excitons) is regarded as equal to the radiative lifetime $\tau_{2r} = \tau_{1r}$ of $S_1$ excitons. Accordingly, we estimate a NR decay rate of $\gamma_{1nr} = \gamma_1 - \gamma_{1r} = 5.65 \times 10^7 s^{-1}$ or a NR lifetime $\tau_{1nr} = 17.5$ ns for the $S_1$ excitons. From the amplitude ratio $\frac{A_1}{A_2} = \frac{n_1(0)}{\tau_{1r}}\frac{\tau_{2r}}{n_2(0)} = 0.57$ at $t = 0$, we find a density ratio of available $S_1$ and $S_2$ states of $n_1^0 : n_2^0 \approx 4 : 7$ at 2.32 eV detection energy, which is a structural quantity of the film being independent of the pump fluence and of the temperature. Time-resolved measurements at various detection energies (not shown here) further reveal a decrease of the faster $S_1$ amplitude with respect to the slower decaying $S_2$ amplitude when the detection energy is reduced, indicating that component $S_2$ possesses a slightly higher trapping energy with respect to the excited "free" Frenkel excitons as compared to states $S_1$.

Subsequently, we analyze the PL trace at 15 K at highest energy fluence (5.1 $\mu J/cm^2$ per pulse), which shows singlet-singlet annihilation. Since $S_1$ excitons in defective traps have a lower occupation density and a reduced exciton diffusion as compared to $S_2$ excitons in ordered traps, we neglect bimolecular quenching between $S_1$ excitons and describe the time dependence of the $S_1$ and $S_2$ states by the differential equations

$$\frac{n_1(t)}{dt} = -\gamma_{1r} n_1(t), \tag{4}$$

$$\frac{n_2(t)}{dt} = -\gamma_{2r} n_2(t) - \frac{1}{2}\gamma_{bq} n_2(t)^2. \tag{5}$$

Here, $\gamma_{bq}$ is the bimolecular quenching coefficient between radiative $S_2$ excitons. Due to the spatial separation of $S_1$ and $S_2$ excitons as well as of $S_2$ and NR states outside the $S_2$ trapping sites, bimolecular quenching is not considered between those states. In addition, bimolecular annihilation between metastable excited states $S_2^*$ before reaching the $S_2$ energy minimum has been neglected. We further assume that autoionization of highly excited $S_2^*$ states after annihilation can be neglected.[43] Accordingly, the time dependence of the $S_1$ and $S_2$ density is approximately given by

$$n_1(t) = n_1(0)\exp(-t/\tau_1), \tag{6}$$

$$\begin{aligned} n_2(t) &= n_2(0)\exp(-t/\tau_{2r}) \\ &\times \left[\frac{\gamma_{2r}}{\gamma_{2r} + n_2(0)\frac{1}{2}\gamma_{bq} - n_2(0)\frac{1}{2}\gamma_{bq}\exp(-t/\tau_{2r})}\right]. \end{aligned} \tag{7}$$

The rate of the emitted photon density is given by

$$\begin{aligned} N_{\text{photon}}(t) &= \gamma_{1r} n_1(t) + \gamma_{2r} n_2(t) \\ &= \gamma_{1r} n_1(0)\exp(-t/\tau_1) + \gamma_{2r} n_2(0)\exp(-t/\tau_{2r}) \\ &\times \left[\frac{\gamma_{2r}}{\gamma_{2r} + n_2(0)\frac{1}{2}\gamma_{bq} - n_2(0)\frac{1}{2}\gamma_{bq}\exp(-t/\tau_{2r})}\right]. \end{aligned} \tag{8}$$

The thick dashed-dotted red line in Fig. 3 shows a fit of the 15 K trace excited at energy fluence of 5.1 $\mu J/cm^2$, where the lifetimes times $\tau_1$ and $\tau_2$ as well as the $n_1(0) : n_2(0)$ ratio have been fixed to 10 and 23 ns and to 4:7, respectively, where saturation effects at this still-moderate pulse fluence have been neglected.

In order to determine the initial densities $n_1(0)$ and $n_2(0)$ and to infer the bimolecular quenching coefficient from Fig. 3, we calculate the average initial density of excited Frenkel excitons according to

$$n_{\text{Frenkel}}(0) = \frac{1}{L} n_{\text{photon}}[1 - \exp(-\alpha L)], \tag{9}$$

with $\alpha$ being $\sim 4 \times 10^6$ $m^{-1}$ (Refs. 36, 43, 46, and 49) and $L = 120$ nm being the thickness of the investigated $Alq_3$ film. The photon density per pulse has been estimated to

$$n_{\text{photon}} = \frac{\phi}{\hbar\omega} \approx 1.1 \times 10^{13}\ cm^{-2}, \tag{10}$$

(using a rectangular beam profile in space) with $\phi$ being the energy fluence per pulse (5.1 $\mu J/cm^2$). Here, $\omega$ is the angular frequency of the incident light, and $a \approx 21$ $\mu$m is the radius of the focused laser spot on the sample which has been determined using the relation for a Gaussian light beam

$$a = \frac{F}{d} \cdot \frac{2\lambda}{\pi}. \tag{11}$$

In Eq. (11), $F = 250$ mm is the focal length of the lens, $d = 3$ mm is the diameter of the incident beam, and $\lambda = 407$ nm is the excitation wavelength. Using Eq. (9), the density of generated mobile quasifree Frenkel excitons calculates to be $n_{\text{Frenkel}}(0) \approx 3.5 \times 10^{17} cm^{-3}$. We further consider that the PL efficiency is reduced to $\sim$40% by NR decay (caused by NR $S_1$ excitons and NR centers) at 15 K at low energy fluence (see Fig. 2). At this low-excitation density, bimolecular quenching between $S_2$ states can be approximately neglected, and the

time-integrated photon density emitted from $S_1$ and $S_2$ excitons is $n_{\text{phe}} = n_1(0)\gamma_{1r}/\gamma_1 + n_2(0)$. By taking into account that the density ratio of $S_1$ and $S_2$ states is ~4:7, we find that $S_1$ and $S_2$ excitons have an average (macroscopic) initial density of $n_1(0) = 0.18 \times n_{\text{Frenkel}}(0)$ and $n_2(0) = 0.32 \times n_{\text{Frenkel}}(0)$. Using these initial densities in Eq. (8) allows us to fit the PL trace in Fig. 3 at a fluence of 5.1 $\mu$J/cm$^2$ with a low-temperature bimolecular quenching coefficient of $\gamma_{bq} = 1.7 \times 10^{-9}$ cm$^3$ s$^{-1}$.

The derived low-temperature quenching coefficient $\gamma_{bq}$ is by one to two orders of magnitude larger than values reported in Refs. 42 and 43 at room temperature. The consideration of a Gaussian profile of the incident laser beam (not described here) would further enhance the quenching coefficient by a factor of approximately three resulting in a value of $\gamma_{bq} \approx 5 \times 10^{-9}$ cm$^3$ s$^{-1}$. Furthermore, the value of $\gamma_{bq}$ has been determined by estimating the radius of the exciting laser beam using Eq. (11), which is a theoretical limit value. The actual radius might be slightly larger, which would lead to a further increase the value of $\gamma_{bq}$.

According to three-dimensional exciton diffusion theory,[50] the annihilation coefficient can be expressed as $\gamma_{bq} = 8\pi D_s r$ with $r \approx 0.8$ nm (Ref. 51) being the nearest neighbor distance of molecules in $Alq_3$ films. The relation provides a diffusion constant of $D_s = 2.5 \times 10^{-3}$ cm$^2$s$^{-1}$ and a diffusion length of $l_d = \sqrt{6 D_s \tau_2} = 190$ nm using a radiative $S_2$ lifetime of $\tau_{2r} = 23$ ns. These high values of $D_s$ and $l_d$ inexplicably deviate from reported diffusion constants ranging from $D_s = 6 \times 10^{-5} \ldots 3 \times 10^{-6}$ cm$^2$s$^{-1}$[37,38,43] and diffusion lengths $l_d$ ranging between 30 and 5 nm.[37,38,43,52,53] We therefore conclude that the observed strong singlet-singlet annihilation in our $Alq_3$ films at 15 K has a different origin than bimolecular quenching at room temperature, which is attributed to three-dimensional diffusion of migrating excitons.[37,38,43] As mentioned earlier, we propose that the bimolecular quenching process in our $Alq_3$ films at low temperatures is caused by interacting excitons that have been trapped in extended potential minima that accommodate several excitons of nearly same energy. Such trapping potentials are generated by local compressive strain and by fluctuating molecular environments at the grain boundaries between $Alq_3$ nanocrystals. An energy fluence of 5.1 $\mu$J/cm$^2$ generates a quasifree Frenkel exciton density of $n_{\text{Frenkel}} \approx 3.5 \times 10^{17}$s$^{-1}$. The average distance between Frenkel excitons at this energy fluence calculates to approximately $10 \times r$ using a nearest molecule neighbor distance of $r \approx 0.8$ nm.[51] It is therefore likely that several Frenkel excitons get trapped within the same potential minimum if molecular ordered areas (nanocrystals) have a length size of a few tens of nanometers. The funneling of excitons into the same trapping site significantly enhances the local (microscopic) $S_2$ exciton density and hence increases the probability of bimolecular annihilation. At an energy fluence of 0.17 $\mu$J/cm$^2$, the average distance between Frenkel excitons increases to $35 \times r$, reducing the likelihood that at least two excitons from adjacent crystalline grains are trapped in the same potential minimum, thus explaining the reduction of singlet-singlet annihilation at very low power levels.

It should be noted that the low-temperature quenching coefficient due to $S_2$ excitons observed in our investigations is not in contradiction with the reported low singlet-singlet annihilation coefficient values at room temperature obtained at 10–100 times higher excitation intensities or energy fluences.[38,39,42,43] Due to $S_2$ state saturation at high excitation densities and thermal activation of $S_2$ excitons into nonquenchable $S_3$ states at higher temperature (which will be discussed in the next subsection), singlet-singlet annihilation due to $S_2$ excitons only partially contributes to the overall quenching effect and singlet-singlet annihilation because of three-dimensional diffusion of migrating excitons becomes the dominant mechanism.

### B. Temperature dependence of the exciton emission

In order to describe the temperature dependence of the PL quenching and the observed redshift of the emission maximum with increasing temperature (see inset of Fig. 1), we extend our set of three exciton states ($S_1$, $S_2$, and NR centers) by thermally activated nonquenchable purely radiative states $S_3$ with additional localization energy $\Delta_l$. As schematically sketched in Fig. 5, these $S_3$ states are located within or in close vicinity to the extended $S_2$ trapping sites but are isolated by a potential barrier of height $\Delta_b$, which is for instance caused by fluctuations in the molecular environment. Here, $S_3$ states could also represent thermally activated CT or excimerlike states where the wave function of the exciton is (at least partially) delocalized between the ligands of two adjacent molecules. As shown for CT and excimer states of stacked PTCDA molecules,[54–56] an additional "self-trapping" energy of ~70 meV is provided by the Coulomb interaction between oppositely charged molecules. Likewise, a potential energy $\Delta_l$ might be generated between oppositely charged ligands of adjacent $Alq_3$ molecules. In both cases, the occupation probability of two adjacent molecules with two excitons is significantly reduced, leading to a decrease of the singlet-singlet annihilation rate and to a redshift of the PL maximum with increasing temperature.

In our model, we assign different localization energies $\Delta_1$, $\Delta_2$, and $\Delta_3$ with respect to the mobile (quasifree) exciton energy to the three sets of radiative exciton states ($S_1$, $S_2$, and $S_3$). We assume a temperature-independent radiative decay rate $\gamma_{fr}$ and capture rate $\gamma_f$ of free excitons, which are generated during the absorption process. We further assume that the radiative rate is much smaller than the capture rate $\gamma_{fr} \ll \gamma_f$ meaning that free excitons are captured within a few hundreds of picoseconds by $S_1$ and $S_2$ states and by NR centers. Accordingly, mobile quasifree excitons only weakly contribute to the total light emission. As mentioned earlier, we consider the rate $\gamma_{fr}$ to be equal to the radiative rate of the trapped states $S_1$ and $S_2$. Furthermore, we assume that the radiative rates $\gamma_{1r}$, $\gamma_{2r}$, and $\gamma_{3r}$ and (background) NR rate $\gamma_{1nr}$ are temperature and excitation-intensity independent. With these assumptions, the rate equations for the exciton states can be given as

$$\frac{dn_f}{dt} = -n_f\gamma_{fr} - n_f\gamma_f + n_1\gamma_f \exp\left(-\frac{\Delta_1}{k_BT}\right) + n_2\gamma_f \exp\left(-\frac{\Delta_2}{k_BT}\right) + n_3\gamma_f \exp\left(-\frac{\Delta_3}{k_BT}\right), \quad (12)$$

$$\frac{dn_1}{dt} = -n_1\gamma_{1r} - n_1\gamma_{1nr} + n_f\gamma_f C_1 - n_1\gamma_f \exp\left(-\frac{\Delta_1}{k_BT}\right), \quad (13)$$

$$\frac{dn_2}{dt} = n_f\gamma_f C_2 - n_2\gamma_{2r} - \frac{1}{2}n_2^2\gamma_{bq} - n_2\Gamma_3(T) - n_2\gamma_f \exp\left(-\frac{\Delta_2}{k_BT}\right) + n_3\Gamma_3(T)\exp\left(-\frac{\Delta_l}{k_BT}\right), \quad (14)$$

$$\frac{dn_3}{dt} = n_2\Gamma_3(T) - n_3\gamma_{3r} - n_3\gamma_f \exp\left(-\frac{\Delta_3}{k_BT}\right) - n_3\Gamma_3(T)\exp\left(-\frac{\Delta_l}{k_BT}\right). \quad (15)$$

Here $n_f$, $n_1$, $n_2$, and $n_3$ are the macroscopic densities of quasifree excitons and of trapped excitons in states $S_1$, $S_2$, and $S_3$, respectively, $k_B$ is the Boltzmann constant. Also, $\Gamma_3(T) = \gamma_{23}\exp(-\frac{\Delta_b}{k_BT})$ is the thermally activated occupation rate of nonquenchable traps $S_3$ with activation energy $\Delta_b$. Constants $C_1 = n_1^0/n_{\rm tot}$ and $C_2 = n_2^0/n_{\rm tot}$ give the ratios of $S_1$ and $S_2$ state densities, respectively, relative to the density of total available trapped states $n_{\rm tot} = n_{\rm NR}^0 + n_1^0 + n_2^0$, which also include the density of NR centers. $\gamma_{bq}$ is the bimolecular annihilation coefficient for $S_2$ states, which is assumed to be temperature and excitation-density independent at applied power levels used in this study. Due to the local separation of $S_1$, $S_2$, and NR states, bimolecular quenching between these states have not been considered. The differential equation for the NR centers $n_{\rm NR}$ containing factor $C_{\rm NR} = n_{\rm NR}^0/n_{\rm tot}$ has been omitted, assuming that these centers do not contribute to the emission of photons due to detrapping at high temperatures. All exciton states are coupled with the mobile Frenkel exciton density by thermal activation (detrapping) into mobile exciton states with rate $\gamma_f$.

For numerical calculations, the decay rates $\gamma_1 = 1\times10^8\ {\rm s}^{-1}$ (with $\gamma_{1r} = 4.35\times10^7\ {\rm s}^{-1}$ and $\gamma_{1nr} = 5.65\times10^7\ {\rm s}^{-1}$) and $\gamma_2 = \gamma_{2r} = 4.35\times10^7\ {\rm s}^{-1}$ of states $S_1$ and $S_2$, respectively, as well as the bimolecular quenching coefficient $\gamma_{bq} = 1.7\times10^{-9}\ {\rm cm}^3\ {\rm s}^{-1}$ has been inferred from the fits in Fig. 3. Also inferred from this fit is the density of states ratio of $n_1^0 : n_2^0 \approx 4:7$. As described earlier, this density ratio and the time-integrated PL efficiency of ~40% at 15 K at low excitation fluence (see Fig. 2) determines the densities of radiative $S_1$ and $S_2$ excitons and of NR excitons to be $n_1(0) = 0.18\times n_{\rm Frenkel}(0)$, $n_2(0) = 0.32\times n_{\rm Frenkel}(0)$, and $n_{\rm NR}(0) = 0.50\times n_{\rm Frenkel}(0)$, respectively. The density of quasifree Frenkel excitons $n_{\rm Frenkel}(0)$ has been calculated according to Eqs. (9)–(11). The radiative decay rate $\gamma_{3r} = 4.0\times10^7\ {\rm s}^{-1}$ of thermally activated nonquenchable $S_3$ states has been deduced from fitting the PL trace at low fluence obtained at 170 K. The radiative decay rate of the quasifree Frenkel excitons $\gamma_{fr} = 4.35\times10^7\ {\rm s}^{-1}$ has been chosen to be equal to the measured radiative rate $\gamma_{2r}$ of states $S_2$.

The observed PL with an emission maximum at ~2.4 eV is attributed to trapped states $S_1$ and $S_2$ with trapping energies of $\Delta_1 = 100$ meV and $\Delta_2 = 110$ meV, respectively. The trapping energies were approximately deduced by comparing the PL maximum at 15 K from crystalline $Alq_3$ samples where the PL is predominantly due to quasifree relaxed Frenkel excitons with the PL maximum from $Alq_3$ films, where the emission is from trapped excitons.[21–23] The higher trapping energy of state $S_2$ compared to $S_1$ is consistent with results from time-resolved PL measurements at different detection energies, as mentioned earlier. The trapping rate $\gamma_f$ of free excitons is connected with the trapping energies $\Delta_1$ and $\Delta_2$ via thermally activated detrapping. The trapping rate $\gamma_f$ has been adjusted to $\gamma_f = 5.88\times10^9\ {\rm s}^{-1}$ to match the 300 K PL traces in Fig. 6.

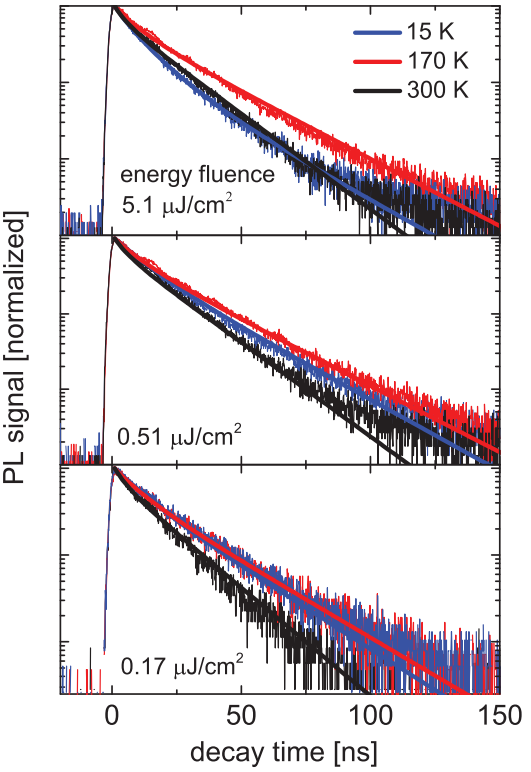


FIG. 6. (Color online) TRPL and normalized PL intensity (thin curves) obtained from a 120 nm $Alq_3$ film at different energy fluences as labeled at temperatures (a) 15, (b) 170, and (c) 300 K. Also shown (thick curves) are calculated PL traces obtained from the rate equation model as explained in the text.

The localization energy $\Delta_l = 45$ meV of the thermally activated nonquenchable state $S_3$ has been deduced from the fact that the PL maximum is shifting by ~25 meV to lower energy when state $S_3$ is occupied (see inset in Fig. 1 at 170 K). Assuming that $S_1$ and $S_2$ states do not possess a significant blueshift due to thermally activated higher vibronic states, the trapping energy of state $S_3$ can be estimated to be $\Delta_3 = \Delta_2 + \Delta_l = 155$ meV to account for the observed redshift of the PL maximum in the inset of Fig. 1. The remaining unknown activation energy $\Delta_b = 20$ meV of states $S_3$ as well as the transition rate $\gamma_{23} = 1\times10^9\ {\rm s}^{-1}$ from state $S_2$ to state $S_3$ are empirically adjusted to generate a reasonable agreement with the experimentally observed PL traces as a function of temperature, as shown in Fig. 6. The used model parameters are summarized in Table I.

Calculated PL traces at an energy fluence of 5.1 $\mu$J/cm$^2$ per pulse and at various temperatures as labeled are shown in Fig. 6(a). Besides the contribution of long-living components, which have been neglected in our model, the calculated (simulated) curves are in good agreement with the experimentally observed PL traces. As expected, the traces show a decreasing

TABLE I. Parameters used to simulate the dynamical behavior of bimolecular annihilation of trapped excitons. Here, $\gamma_f$ is the trapping rate from free excitons; $\gamma_{fr}$, $\gamma_{1r}$, $\gamma_{2r}$, and $\gamma_{3r}$ are the radiative rates of free excitons and of $S_1$, $S_2$, and $S_3$ states, respectively; $\gamma_{1nr}$ is the NR rate of state $S_1$. Also, $\gamma_{23}$ and $\gamma_{bq}$ are the transition rate from state $S_2$ to $S_3$ excitons and bimolecular quenching rate of state $S_2$, respectively. Then $\Delta_1$, $\Delta_2$, and $\Delta_3$ are localization energies of states $S_1$, $S_2$, and $S_3$. Energies $\Delta_b$ and $\Delta_l$ denote the thermal activation and localization energies of the $S_3$ state, respectively.

| | |
|---|---|
| $\gamma_f$ | $5.88 \times 10^9$ s$^{-1}$ |
| $\gamma_{fr}$ | $4.35 \times 10^7$ s$^{-1}$ |
| $\gamma_{1r}$ | $4.35 \times 10^7$ s$^{-1}$ |
| $\gamma_{2r}$ | $4.35 \times 10^7$ s$^{-1}$ |
| $\gamma_{3r}$ | $4.00 \times 10^7$ s$^{-1}$ |
| $\gamma_{1nr}$ | $5.65 \times 10^7$ s$^{-1}$ |
| $\gamma_{23}$ | $1 \times 10^9$ s$^{-1}$ |
| $\gamma_{bq}$ | $1.7 \times 10^{-9}$ cm$^3$s$^{-1}$ |
| $\Delta_1$ | 100 meV |
| $\Delta_2$ | 110 meV |
| $\Delta_3$ | 155 meV |
| $\Delta_b$ | 20 meV |
| $\Delta_l$ | 45 meV |

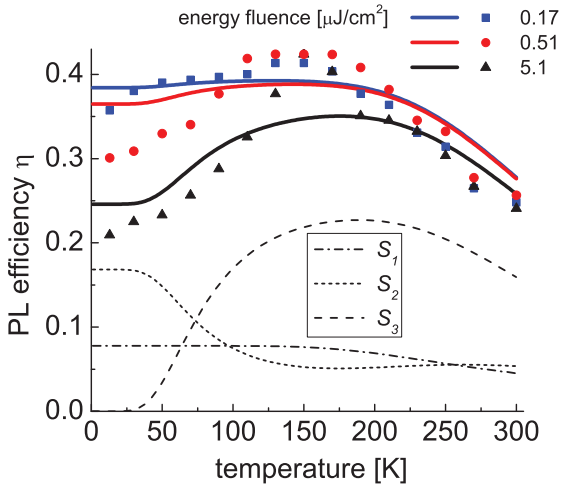


FIG. 7. (Color online) Calculated total time-integrated PL efficiency as a function of temperature for different energy fluences as labeled. Also shown are individual contributions from states $S_1$, $S_2$, and $S_3$ to the light emission at an energy fluence of 5.1 $\mu$J/cm$^2$ per pulse. For comparison, the experimentally obtained PL efficiency values from Fig. 2 are inserted as symbols.

contribution of bimolecular quenching with increasing temperature due to the occupation of nonquenchable states $S_3$. At higher temperatures, the decay rate increases due to a thermal activated detrapping of all radiative states and subsequent filling of NR traps via mobile Frenkel excitons.

Calculated PL traces at 0.51 and 0.17 $\mu$J/cm$^2$ and at 15, 170, and 300 K are shown in Figs. 6(b) and 6(c). They show a weaker contribution of bimolecular quenching, which is particularly noticeable at an energy fluence of 0.17 $\mu$J/cm$^2$, where the PL traces at 15 and 190 K are almost identical. At higher temperatures (and nearly independent of the excitation power), the decay rate increases due to thermal activation of radiatively emitting states and subsequent filling of NR trapped states, as mentioned before.

### C. Time-integrated PL efficiency

Finally, we calculated the time-integrated density of emitted photons $n_{\rm phe}(T)$ from trapped states $S_1$, $S_2$, as well as from the $S_3$ states according to

$$n_{\rm phe}(T) = \int_0^\infty \gamma_{1r} n_1(t,T)dt + \int_0^\infty \gamma_{2r} n_2(t,T)dt + \int_0^\infty \gamma_{3r} n_3(t,T)dt. \quad (16)$$

In these calculations, we neglected the weak contribution of quasifree excitons to the light emission due to their fast capture rate $\gamma_f$. The results are depicted in Fig. 7 for different energy fluences. Shown are the calculated total time-integrated PL efficiencies as a function of temperature for energy fluences of 5.1, 0.51, and 0.17 $\mu$J/cm$^2$, respectively, as well as the individual contributions from states $S_1$, $S_2$, and $S_3$ at an energy fluence of 5.1 $\mu$J/cm$^2$ per pulse. For comparison, the experimentally obtained efficiency values from Fig. 2 have been inserted in Fig. 7. As for the time-resolved traces in Fig. 6, the calculated total time-integrated PL efficiencies essentially reproduce the temperature-dependent behavior of the experimental data at different excitation densities. Deviations at low temperature are predominantly attributed to the disregard of bimolecular quenching of excitons during the filling process of $S_2$ states into the trapping site, where the microscopic density is already high. This effect reduces the trapped initial $S_2$ density and hence decreases the PL intensity at higher excitation levels, which is currently not included in our model.

## V. SUMMARY

Time-integrated and time-resolved PL measurements of thin OMBD-grown $Alq_3$ films show an increase of the PL efficiency when the temperature is increased from 15 to ~170 K. Above 170 K, the intensity and the decay rate of the PL emission decreases. Intensity-dependent measurements show that the reduction of the PL efficiency below 170 K is caused by singlet-singlet annihilation. The extracted low-temperature bimolecular annihilation coefficient at 15 K has been estimated to be $\gamma_{bq} = 1.7 \times 10^{-9}$ cm$^3$ s$^{-1}$ using a rectangular beam profile in space. Considering a Gaussian profile of the incident laser beam, the quenching coefficient increases to $\gamma_{bq} \approx 5 \times 10^{-9}$ cm$^3$ s$^{-1}$, which is more than two orders of magnitude larger than values reported earlier.[38,39,42] The high quenching rate at 15 K is explained by a directed migration of mobile Frenkel excitons, which are generated in short-range crystalline grains in the polycrystalline film into extended trapping areas with low-defect density at grain boundaries. The capture of excitons at such trapping sites significantly enhances the local (microscopic) exciton density, leading to intense bimolecular quenching already at moderate excitation densities. The observed reduction of annihilation between trapped singlet excitons with increasing temperature is attributed to a thermally activated occupation of nonquenchable states, including isolated traps or CT-like

states. Above 170 K, the PL efficiency decreases, which is attributed to a detrapping of excitons and subsequent filling of NR traps, which is consistent with earlier interpretations.[38]

The experimental results have been modeled using coupled-rate equations, which include bimolecular quenching, thermally activated occupation of nonquenchable states, and thermally activated detrapping of excitons at higher temperatures. Despite the complexity of the exciton dynamics and our simplifying assumptions, the theoretical results are in good agreement with the experimental findings. Though bimolecular quenching by trapped $S_2$ excitons is significantly reduced at higher temperatures due to thermal activation into $S_3$ excitons, it is still active at room temperature. This might explain the differences of diffusive annihilation coefficients obtained from $Alq_3$ films that were grown at different growth conditions.[38,39,42,43] We expect that the contribution of singlet-singlet annihilation by trapped excitons at grain boundaries decreases when the size of molecularly ordered areas in $Alq_3$ films decreases or equivalently when the degree of molecular disorder increases. Studying bimolecular quenching as a function of molecular order by fabricating $Alq_3$ films at different growth conditions, for instance by changing the substrate temperature, will be the subject of further investigations.

## ACKNOWLEDGMENT

The authors are indebted to V. R. Gangilenka for his experimental support and his helpful discussions.

*Corresponding author: wagnerhp@uc.edu

[1] C. W. Tang and S. A. Van Slyke, Appl. Phys. Lett. **51**, 913 (1987).
[2] P. E. Burrows, V. Bulovic, S. R. Forrest, L. S. Sapochak, D. M. McCarty, and M. E. Thompson, Appl. Phys. Lett. **65**, 2922 (1994).
[3] J. Kalinowski, P. DiMarco, M. Cocchi, V. Fattori, N. Camaioni, and J. Duff, Appl. Phys. Lett. **68**, 2317 (1996).
[4] A. Dodabalapur, Solid State Commun. **102**, 259 (1997).
[5] S. W. Wen, M. T. Lee, and C. H. Chen, IEEE J. Display Technol. **1**, 90 (2005).
[6] W. Li, A. Jones, S. C. Allan, J. C. Heikenfeld, and A. J. Steckl, IEEE J. Display Technol. **2**, 143 (2006).
[7] L. S. Hung, C. W. Tang, and M. G. Mason, Appl. Phys. Lett. **70**, 152 (1997).
[8] L. S. Hung, C. W. Tang, M. G. Mason, P. Raychaudhuri, and J. Madathil, Appl. Phys. Lett. **78**, 544 (2001).
[9] M. G. Mason, C. W. Tang, L. S. Hung, P. Raychaudhuri, J. Madathil, D. J. Giesen, L. Yan, Q. T. Le, Y. Gao, S. T. Lee, L. S. Liao, L. F. Cheng, W. R. Salaneck, D. A. dos Santos, and J. L. Bredas, J. Appl. Phys. **89**, 2756 (2001).
[10] J. Cui, Q. L. Huang, J. G. C. Veinot, H. Yan, and T. J. Marks, Adv. Mater. **14**, 565 (2002).
[11] T. J. Marks, J. G. C. Veinot, J. Cui, H. Yan, A. Wang, N. L. Edleman, J. Ni, Q. Huang, P. Lee, and N. R. Armstrong, Synth. Met. **29**, 29 (2002).
[12] S. Wang, Y. Q. Liu, X. B. Huang, S. L. Xu, J. R. Gong, X. H. Chen, L. Yi, Y. Xu, G. Yu, L. J. Wan, C. L. Bai, and D. B. Zhu, Appl. Phys. A **78**, 553 (2004).
[13] D. U. Lee, Y. B. Yoon, S. H. Baek, T. W. Kim, J. H. Seo, and Y. K. Kim, Thin Solid Films **516**, 3627 (2008).
[14] E. M. Han, L. M. Do, N. Yamamoto, and M. Fujihira, Thin Solid Films **273**, 202 (1996).
[15] E. M. Han, L. M. Do, N. Yamamoto, and M. Fujihira, Mol. Cryst. Liq. Cryst. Sci. Technol., Sec. A **280**, 349 (1996).
[16] H. Aziz, Z. Popovic, S. Xie, A. M. Hor, N. X. Hu, C. Tripp, and G. Xu, Appl. Phys. Lett. **72**, 756 (1998).
[17] C. Y. Kwong, A. B. Djurisic, W. C. H. Choy, D. Li, M. H. Xie, W. K. Chan, K. W. Cheah, P. T. Lai, and P. C. Chui, Mater. Sci. Eng. B **116**, 75 (2005).
[18] V. K. Shukla, S. Kumar, and D. Deva, Synth. Met. **156**, 387 (2006).
[19] F. J. Zhang, Z. Xu, D. W. Zhao, S. L. Zhao, W. W. Jiang, G. C. Yuan, D. Song, Y. S. Wang, and X. R. Xu, J. Phys. D **40**, 4485 (2007).
[20] G. F. Wang, X. M. Tao, and H. M. Huang, Appl. Surf. Sci. **253**, 4463 (2007).
[21] M. Brinkmann, G. Gadret, M. Muccini, C. Taliani, N. Masciocchi, and A. Sironi, J. Am. Chem. Soc. **122**, 5147 (2000).
[22] M. Brinkmann, G. Gadret, C. Taliani, N. Masciocchi, A. Sironi, and M. Muccini, Synth. Met. **121**, 1499 (2001).
[23] M. Muccini, M. Brinkmann, G. Gadret, C. Taliani, N. Masciocchi, and A. Sironi, Synth. Met. **122**, 31 (2001).
[24] M. Braun, J. Gmeiner, M. Tzolov, M. Coelle, F. D. Meyer, W. Milius, H. Hillebrecht, O. Wendland, J. U. von Schutz, and W. Brutting, J. Chem. Phys. **114**, 9625 (2001).
[25] M. Rajeswaran and T. N. Blanton, J. Chem. Crystallogr. **35**, 71 (2005).
[26] C. Ghica, M. N. Grecu, J. Gmeiner, and V. V. Grecu, J. Optoelectronics Adv. Mater. **7**, 2997 (2005).
[27] M. D. Halls and H. B. Schlegel, Chem. Mater. **13**, 2632 (2001).
[28] P. E. Burrows and S. R. Forrest, Appl. Phys. Lett. **64**, 2285 (1994).
[29] S. K. Saha, Y. K. Su, and E. S. Juang, IEEE J. Quantum Electron. **37**, 807 (2001).
[30] I. Hernandez, W. P. Gillin, and M. Somerton, J. Lumin. **129**, 1835 (2009).
[31] A. Y. Kobitski, R. Scholz, I. Vragovic, H. P. Wagner, and D. R. T. Zahn, Phys. Rev. B **66**, 153204 (2002).
[32] A. Y. Kobitski, R. Scholz, D. R. T. Zahn, and H. P. Wagner, Phys. Rev. B **68**, 155201 (2003).
[33] H. P. Wagner, V. R. Gangilenka, A. DeSilva, H. Schmitzer, R. Scholz, and T. U. Kampen, Phys. Rev. B **73**, 125323 (2006).
[34] H. P. Wagner, A. DeSilva, and T. U. Kampen, Phys. Rev. B **70**, 235201 (2004).
[35] G. Y. Zhong, X. M. Ding, J. Zhou, N. Jiang, W. Huang, and X. Y. Hou, Chem. Phys. Lett. **420**, 347 (2006).
[36] A. D. Walser, I. Sokolik, R. Priestly, and R. Dorsinville, Appl. Phys. Lett. **69**, 1677 (1996).
[37] I. Sokolik, R. Priestley, A. D. Walser, R. Dorsinville, and C. W. Teng, Appl. Phys. Lett. **69**, 4168 (1996).
[38] A. D. Walser, R. Priestley, and R. Dorsinville, Synth. Met. **102**, 1552 (1999).
[39] I. Sokolik, A. D. Walser, R. Priestley, C. W. Tang, and R. Dorsinville, Synth. Met. **84**, 921 (1997).

[40]W. Humbs, H. Zhang, and M. Glasbeek, Chem. Phys. **254**, 319 (2000).
[41]K. Thangaraju, J. Kumar, P. Amaladass, A. K. Mohanakrishnan, and V. Narayanan, Appl. Phys. Lett. **89**, 082106 (2006).
[42]R. Priestley, A. D. Walser, and R. Dorsinville, Opt. Commun. **158**, 93 (1998).
[43]J. Mezyk, J. Kalinowski, F. Meinardi, and R. Tubino, Chem. Phys. Lett. **395**, 321 (2004).
[44]V. Kishore, K. L. Narasimhan, and N. Periasamy, Phys. Chem. Chem. Phys. **5**, 1386 (2003).
[45]Y. Kawamura, H. Sasabe, and C. Adachi, Jpn. J. Appl. Phys. **43**, 7729 (2004).
[46]D. Z. Garbuzov, S. R. Forrest, A. G. Tsekoun, P. E. Burrows, V. Bulovic, and M. E. Thompson, J. Appl. Phys. **80**, 4644 (1996).
[47]H. Mattoussi, H. Murata, C. D. Merritt, Y. Iizumi, J. Kido, and Z. H. Kafafi, J. Appl. Phys. **86**, 2642 (1999).
[48]M. Coelle, C. Gaerditz, and A. G. Mueckl, Synth. Met. **147**, 97 (2004).
[49]C. Himcinschi, N. Meyer, S. Hartmann, M. Gersdorff, M. Friedrich, H. H. Johannes, W. Kowalsky, M. Schwambera, G. Strauch, M. Heuken, and D. R. T. Zahn, Appl. Phys. A **80**, 551 (2005).
[50]V. K. Brikenshtein, V. A. Benderskii, and P. G. Filippov, Phys. Status Solidi B **117**, 9 (1983).
[51]G. G. Malliaras, Y. L. Shen, D. H. Dunlap, H. Murata, and Z. H. Kafafi, Appl. Phys. Lett. **79**, 2582 (2001).
[52]C. W. Tang, S. A. Vanslyke, and C. H. Chen, J. Appl. Phys. **65**, 3610 (1989).
[53]J. Kalinowski, V. Fattori, and P. Di Marco, Chem. Phys. **266**, 85 (2001).
[54]R. Scholz, A. Y. Kobitski, D. R. T. Zahn, and M. Schreiber, Phys. Rev. B **72**, 245208 (2005).
[55]V. R. Gangilenka, A. DeSilva, H. P. Wagner, R. E. Tallman, B. A. Weinstein, and R. Scholz, Phys. Rev. B **77**, 115206 (2008).
[56]V. R. Gangilenka, L. V. Titova, L. M. Smith, H. P. Wagner, L. A. A. DeSilva, L. Gisslen, and R. Scholz, Phys. Rev. B **81**, 155208 (2010).